JOURNAL OF PROPULSION AND POWER
Vol. 18, No. 1, January–February 2002

Flow Control via Rotor Trailing Edge Blowing in Rotor/Stator Axial Compressor

A. M. Wo,* A. C. Lo,† W. C. Chang‡
National Taiwan University, Taipei 106, Taiwan, Republic of China

An experimental study is presented of flow control of the rotor wake in a rotor/stator axial compressor. The objective is to quantify the reduction in the stator forced response due to flow blowing from the rotor trailing edge. The experiment was conducted in a low-speed, large-scale axial compressor at both near-design and high time-mean blade loading. The blowing cases considered are 35, 72, and 105% of the nonblowing wake momentum defect, which ranges from 1.3 to 3.7% of the compressor mass flow at near-design loading. Instrumentation include slanted hot wire to acquire three-dimensional ensemble-averaged rotor wake profile and fast-response pressure gauges embedded within the stator blades at midspan. Results show that the development of the near wake (15% chord downstream of trailing edge) is very much loading dependent; the same amount of blowing momentum has an effect on the velocity defect at near-design loading but not at high loading. Farther downstream, trailing-edge blowing is effective in energizing the wake. The decrease in magnitude of transverse gust is essentially linear with the wake momentum increase due to the blowing flow. Data show reduction in the stator unsteady force amplitude for all blowing cases tested. With the wake momentum at 72% of that for the wakeless flow, force amplitude reduction of 25 and 35% are realized for the near-design and high loading cases, respectively.

I. Introduction

WAKES from blades are a fact of life. As a natural consequence of boundary layers from blade surfaces, a wake is problematic. It robs energy from the outer flow for its own gain, lowering the efficiency of turbomachines. Noise, a result of wake/blade interaction, can propagate to cause nuisance if not properly designed for. Blade vibration, due to forced response of the passing wake, may lead to high cycle fatigue and eventual disastrous blade failure.

Several studies[1–5] were made on wake control strategies relevant to compressor and fan blades. Kerrebrock et al.,[2] primarily focusing on performance enhancement, advocated the use of suction to remove flow just before substantial rise in pressure, that is, where the boundary layer begins to grow substantially, which resulted in significant increase in diffusion and work done per stage. This concept also provides a thermodynamic benefit by removing the high-entropy fluid from the flow path. A family of fan stages of varying tip speed was also studied using quasi-viscous and three-dimensional Euler computational tools. Rao et al.[3] conducted an experimental investigation to reduce the unsteady stator/rotor interaction in a turbofan simulator using microelectromechanical system- (MEMS-) based active flow control. The fan rotor of a $\frac{1}{14}$-scale turbofan propulsion simulator is subjected to circumferentially periodic inlet flow distortions. The stator wakes are reenergized by injecting air from the trailing edge of each stator through discrete blowing holes. The flow rate through each blowing hole is controlled by an individual MEMS microvalve. This work demonstrated the feasibility and advantage of active control by the ability of the system to respond to changes in the inlet flow velocity. Valkov and Tan[4] studied wake/stator interaction via spectral methods and showed excellent spatial resolution of the flow structure. The interaction produces convecting vortical disturbances within the stator passage, which correlates well with the surface pressure fluctuations. The wakes migrate toward the pressure surface where they evolve into counter-rotating vortices. These vortices are the dominant source of disturbances over the pressure surface of the stator blade. Waitz et al.[5] assessed the wake generated noise with and without various means of flow control. Both computational work and cascade experiments were executed. The study found that greater than 40% reduction of wake deficit and greater than 35% reduction of unsteady velocity fluctuations can be realized by suction of less than 3% of fan throughflow or blowing of less than 1% of fan throughflow via the blade trailing edge. Reduction of mode amplitude of 4 dB with suction was achieved or 4–11 dB with blowing.

This work focuses on wake control for the purpose of reducing the forced response on downstream blade rows in an axial flow compressor. Manwaring and Wisler[6] assessed various state-of-the-art computational tools to predict gust response in compressors and turbines, which clearly showed the importance of the wake in light of issues related to forced response. An earlier work, Hsu and Wo[7] (based on the gust decomposition methodology of Wo et al.[8]), demonstrated that for a rotor/stator/rotor configuration, clocking of the rotor rows can substantially offset the stator forced response due to the upstream rotor wake by the influence of the downstream rotor row. For one case tested, a 60% unsteady force reduced was achieved. Although this method of clocking poses no restriction on the rotor/stator blade count ratio, the blade counts for both rotor rows need to be the same for maximum reduction of forced response on the stator. The present study deals directly with the wake, and its consequences, by blowing from the rotor trailing edge (see Fig. 1) using a large-scale rotating axial compressor rig. Knowledge of the consequence of a particular wake profile on the response of the downstream blade is deemed beneficial from a design point of view even though this method of flow control may or may not be directly utilized.

II. Approach

A three-step approach is adopted. First, to characterize the rotor wake three-dimensional ensemble-averaged velocities with and without blowing is measured via a slanted hot wire located at three downstream locations and two time-mean loadings. Second, with the wake data, the transverse gust v^+ acting on the downstream stator is calculated. This provides a qualitative indication of the effect of flow control on the stator response because, the axial spacing in this work being 30% chord, the contribution from the rotor potential field toward the stator response is much less than the rotor vortical

Received 1 December 2000; revision received 6 July 2001; accepted for publication 13 July 2001.

*Professor, Institute of Applied Mechanics; andrew@iam.ntu.edu.tw.
†Graduate Student, Institute of Applied Mechanics.
‡Graduate Student, Institute of Applied Mechanics.

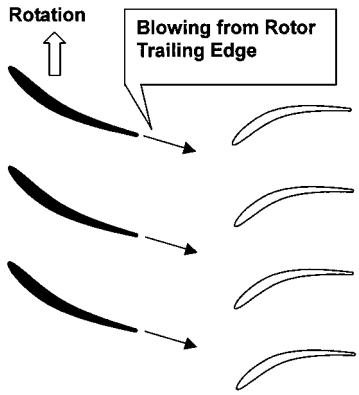

Fig. 1 Blowing flow from the rotor trailing edge in a rotor/stator axial compressor.

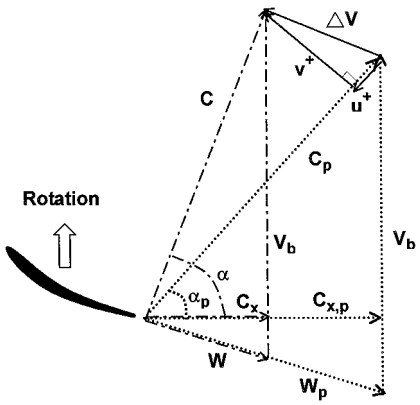

Fig. 2 Velocity triangle in the rotor wake.

field.[7] Third, the effect of energized wake on stator unsteady response is quantified via unsteady pressure data on blade surfaces. All data are taken at the blade midspan location.

III. Gust and Blowing Considerations

We will now define two parameters that will be used throughout the paper. The gust factor provides an idea of how the flow control strategy affects the stator unsteady loading based on the wake data alone. To this end, one can consider the flow kinematics involved. Figure 2 shows the velocity triangle at a point downstream of the rotor. Three sets of velocity triangles are shown: 1) the dotted lines represent velocities outside of the wake vortical region, 2) the dot–dash lines represent velocities within the wake, and 3) the solid lines are the streamwise and transverse gusts u^+ and v^+, respectively, which act on the downstream stator. C is the absolute velocity, W the relative velocity, and V_b the blade speed. Subscript x is the axial direction and subscript p the wake velocity outside the vertical region. The dominant contribution to stator unsteadiness is due to the transverse gust. The transverse gust (see Fig. 2) can be written as

$$v^+ = C\sin(\alpha - \alpha_p) \tag{1}$$

Expanding the sine term and using $C = Cx/(\cos a)$ results in

$$v^+ = C_x(\tan\alpha\cos\alpha_p - \sin\alpha_p) \tag{2}$$

Define a gust factor G to characterize the overall level of gust that the downstream stator experiences over an unsteady cycle T, that is,

$$G \equiv \frac{\int_0^T v^+\,\mathrm{d}t}{\int_0^T v_0^+\,\mathrm{d}t} \tag{3}$$

where the subscript 0 represents the no blowing case. Hence, the gust factor G is unity (maximum gust) without flow control and zero (minimum gust) when control is applied so that v^+ vanishes over a period. Substituting Eq. (2) into Eq. (3), one obtains

$$G \equiv \frac{\int_0^T C_x(\tan\alpha\cos\alpha_p - \sin\alpha_p)\,\mathrm{d}t}{\int_0^T C_{x,0}(\tan\alpha\cos\alpha_p - \sin\alpha_p)\,\mathrm{d}t} \tag{4}$$

Equation (4) assumes that the angles α and α_p remain essentially unchanged with and without flow control, which should be valid for the same time-mean blade loading.

To quantify the degree that the blowing flow energizes the wake it is intuitive to define a wake momentum defect factor as

$$K_m \equiv \frac{\int_{\text{wake}} \rho\left(W^2 - W_0^2\right)\mathrm{d}y}{\int_{\text{wake}} \rho\left(W_p^2 - W_0^2\right)\mathrm{d}y} \tag{5}$$

where W is the rotor relative velocity and the subscripts 0 and p represent the no blowing flow and the wake outer flow, respectively. The integration is carried out in the tangential (blade-to-blade) direction over the entire wake. The Mach number based on the wake outer flow W_P is 0.09, hence, density variation is negligible. Physically, K_m equals zero for the no blowing case and unity when the energized wake acquires the same momentum as the wakeless flow, a uniform flow with the same velocity as the wake outer flow.

IV. Experimental Aspects

A. Axial Compressor Rig

The experimental compressor is a low-speed, large-scale, one-to-three stage rig, designed after modern compressors (Fig. 3) (Table 1 and the Appendix of Hsu and Wo[7] provide more details on the compressor and the blade coordinates as well). Two special features are designed in the rig: The axial spacing between blade rows are variable, from 10 to 60% chord, and the clocking position between rotor rows can be adjusted.

The blades were designed using controlled diffusion concept of Hobbs and Weingold.[9] The inlet guide vane (IGV)/rotor/stator count is 60/58/60, with all blades having a chord of 6 cm. The IGV trailing edge is located 1.75 chords upstream of the rotor leading edge to allow for wake dissipation. (Less than 2% of the lightly loaded IGV wake defect can be felt at the rotor inlet.) The rotor rotates at 1050 rpm with a midspan speed, V_b, of 44.53 m/s. In this work, the axial spacing between the rotor and stator is set at 30% chord, and two time-mean blade loading are tested: near-design ($C_x/V_b = 0.60$) and high loading ($C_x/V_b = 0.53$). For the rotor wake measurement, the stator leading edge was two chords downstream of the rotor trailing edge; thus, the stators do not influence the rotor wake.[10] The measured rotor/stator static-to-static pressure rise characteristic (see Fig. 3 of Hsu and Wo[7]) is representative of highly loaded blade of modern compressor design.

Supply of laboratory compressed air to the rotor with trailing-edge blowing is accomplished through the compressor main shaft. At the time of initial compressor design, this experiment was already conceived; thus, the shaft was made hollow with various openings on the shaft wall (holes drilled radially). Compressed air from storage tank is routed to the front cone (see Fig. 3) through a center hole and is connected to the shaft via a homemade slip ring. This is essentially a ball bearing with the outer cage press-fit into the hollow shaft and the inner cage tightly holding the supply air hose. A seal at the inner face (high-pressure end) of the bearing prevents supply air leaking through the balls.

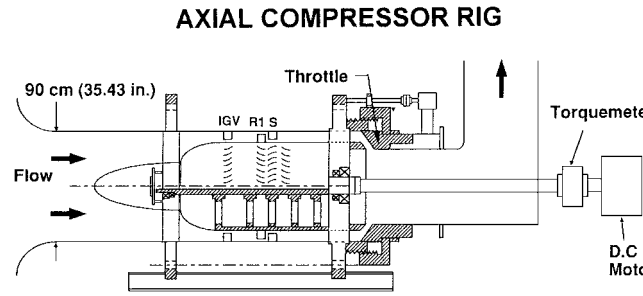

Fig. 3 Axial compressor rig used (further details are provided by Hsu and Wo[7]).

B. Instrumentation

The unsteady pressure on the stator suction and pressure surfaces were measured using fast-response pressure transducers (Kulite LQ-125), which were embedded within two adjacent blades (10 transducers per surface along the midspan). The isolated transducer alone dominated the system response, as calculated from Doebelin.[11] Transducer signals of 128 data points in a rotor blade-to-blade period were acquired per shaft revolution. The pressure transducer is a gauge type with the atmospheric pressure as the sealed reference pressure. The output signal was connected to a low-noise amplifier (Stanford Research SR560) as a differential signal, that is, the positive output subtracts the negative output within the amplifier, then digitized with a 12-bit analog-to-digital resolution. The accuracy of the surface pressure measurement is ±3% determined from calibration.

To provide timing information, a photosensitive diode was used to sense the passing of a metal protrusion rotating with the shaft, with a timing accuracy of 0.1% of a blade-to-blade period. Therefore, data from the same rotor wake were recorded. The time $t = 0$ corresponds to the instant when the trailing edge of the rotor, whose wake is to be measured throughout, is axially upstream of the leading edge of the stator blade with pressure transducers instrumented on the suction surface. Because pressure transducers are mounted on two adjacent stator blades, data acquisition on the stator pressure surface was delayed one unsteady cycle. To preserve the time series, an analog filter was not used before digitization, but the signal was monitored using a spectrum analyzer (Hewlett-Packard 3561A); no high-frequency content exists that could alias the blade-to-blade frequency and next few higher modes. Moreover, a phase-locked averaging technique was also used to filter non-blade-to-blade periodic signals (240 typical ensembles were used).

Hsu and Wo[12] provide details on gust measurement using the slanted hot-wire technique, with an accuracy from calibration of ±1% in magnitude and ±1.5 deg in flow angles. A total of 197 points are collected per rotor pitch for each trigger (one ensemble) and 1000 ensembles are acquired for the same wake.

C. Blowing Considerations

The dominant reason for the instrumented rotor for flow control instead of the stator was the uncompromising desire to obtain accurate unsteady surface pressure data via miniature Kulite pressure transducers (Model LS-125, 5 psi differential) embedded within either the rotor or the stator. Because the unsteady pressure signal is expected to be small (about 10 millivolt raw signal), mounting the transducers on the rotor would require a slip ring, or a complex telemetry system, which would have added an unknown amount of noise depending on the type of rotating to stationary system used. This approach is deemed too risky from the outset of the experiment. Mounting the pressure transducers on the stator, however, would require a slip ring to deliver compressed air from the laboratory to the injection point on the rotor, which can be overcome without penalty or risk on data quality. Thus, the surface pressure data on the stator were taken. At the near-design point, the blowing mass flow is 1.3% of the passage throughflow for $K_m = 0.35$ and 3.7% for $K_m = 1.05$.

The design of rotor blade internal passages for uniform blowing at the trailing edge was achieved with great difficulty. The blade needs to be hollowed out to allow the blowing flow to enter the blade from the root, then turn 90 deg toward the trailing edge. This must be accomplished with sufficient structural integrity remaining for the rotating blade and to achieve uniform flow at the trailing-edge exit. Three designs were fabricated and tested, each with the same slot dimension of 0.8 mm width and 20 mm spanwise centered about the midspan (blade span is 88.8 mm). The three designs differ in the blade internal flow passage. First, borrowing idea from conventional diffuser design, the diffuser design uses vanes to separate the hollowed space into approximately equal area passages. After much effort in tuning the passages with curved vanes, this design is abandoned because strong a three-dimensional effect within the passage prevents a desired flow uniformity at the trailing-edge exit. Second, the tubing design aims to attain uniform exit flow at the expense of increased pressure loss. Tubings of equal length are placed from the rotor root to the trailing edge, with each tube lying flat within the blade structure except near the root. This, however, leads to each tube having a different radius of curvature when turning toward the trailing edge. Measurement of velocity profile aft of the trailing edge, with the instrumented rotor nonrotating, shows the overall flow uniformity is improved over that of the diffuser design. However, nonuniformity due to tubing wall boundary layer is evident at the downstream location that corresponds to the stator leading edge for axial spacing of 10% chord.

The truncated tubing design runs stainless tubing from the root and terminating 5 mm from the trailing edge, with the subsequent void space allowing the tube wall boundary layers to mix before leaving the blade. Measurement of blade exit flow profile 6 mm (10% chord) downstream from the trailing edge show that the root mean square of the time mean axial velocity is 0.7% over the central 4-mm spanwise region and 4.0% over the wider 15-mm range (beyond this range, the effect of the two slot ends becomes evident). Unlike the earlier design, the boundary layers from individual tubes are clearly absent. This excellent flow uniformity was achieved painstakingly by a trial-and-error process of inserting 5–20 mm length of plastic tubings at the entrance of a stainless tube (near the blade root) for the region corresponding to excessive flow. In other words, increase the viscous loss along the particular stainless steel tube that would otherwise result in a high-velocity flow. A total of three such blades are fabricated and mounted in the compressor rig.

The mass flow injected for $K_m = 0.35$ is 1.3% of the blade-to-blade passage flow at near-design loading and 1.2% at high loading. At $K_m = 1.05$, the mass flow is 3.7% at near-design and 3.3% at high loading.

V. Results and Discussion

A. Rotor Wake Velocity Profile

Data of the rotor wake with and without blowing flow will first be presented. Wake profiles at three locations, 15% chord, 30% chord, and 60% chord, downstream of the rotor trailing edge are measured. These locations are chosen because the wakes measured characterize the gust on the closely coupled, downstream stator blades. The blowing cases considered correspond to $K_m = 0, 0.35, 0.72$, and 1.05 for near-design loading and $K_m = 0$, 0.35, and 0.72 for high loading cases, because $K_m = 1.05$ is a high loading case out of the range of slanted hot-wire calibration (the iteration procedure diverged when solving for the velocity data).

Figure 4 presents the wake axial velocity at near-design loading ($C_x / V_b = 0.60$). The abscissa represents the instant when the wake sweeps pass the hot wire. Figure 4a shows the wake profile at 15% chord aft of the trailing edge. The uncontrolled wake result ($K_m = 0$ represents the no blowing case) shows the largest velocity defect compared to other blowing cases, as might be expected. The spike at the left side (pressure surface side) of the velocity profile for the energized wake of $K_m = 1.05$ is the signature of the blowing flow, or due to its momentum surplus. There are two sources that contribute to the bias of the blowing flow toward the pressure surface side of the wake: 1) The blowing air slot is fabricated principally along the camber line near the trailing edge; however, angular variation is difficult to confirm. 2) The presence of flow deviation for a loaded blade would shift the entire wake toward the suction side. The first reason alone might cause the spike to bias toward the pressure surface, but the flow deviation further aggravates this situation. It is reasonable to believe that if the blowing slot were vectored toward the suction boundary layer or even placed on the suction surface, an increased rate of mixing would be achieved. Nevertheless, the blowing spike, which is an unwanted source of gust, only appears at fairly large injection flow and all blowing flows resulted in a lowered maximum velocity defect. This suggests that this form of blowing control in itself is effective regardless of fine details of the blowing slot design.

The development of the wake farther downstream is shown in Figs. 4b and 4c. Figure 4b shows similar trend at 30% chord aft,

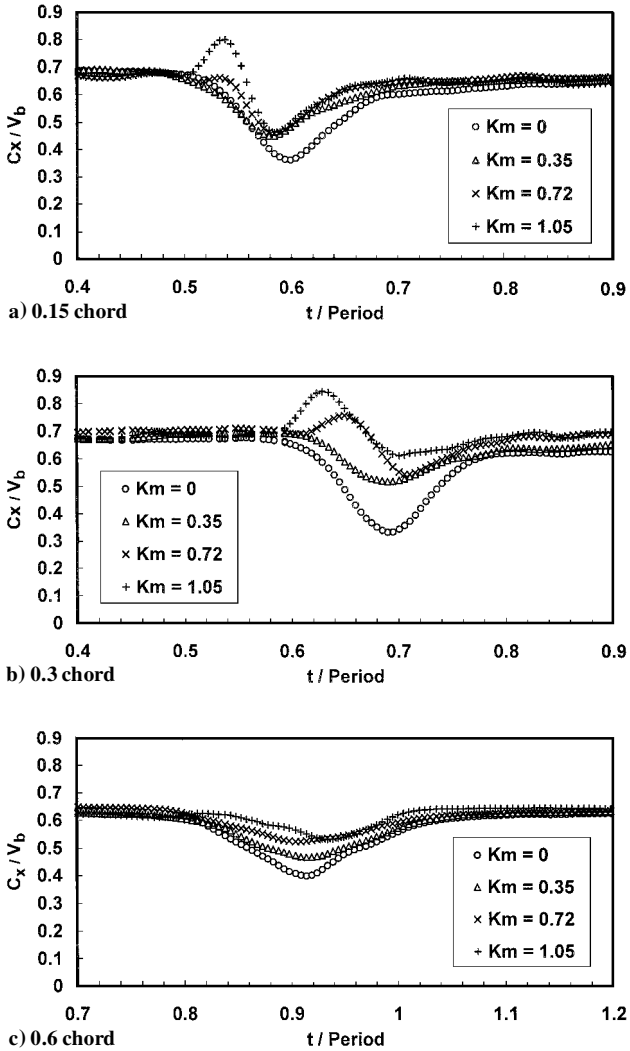

Fig. 4 Measured axial velocity wake profile with hot wire located aft of the rotor trailing edge at near-design loading.

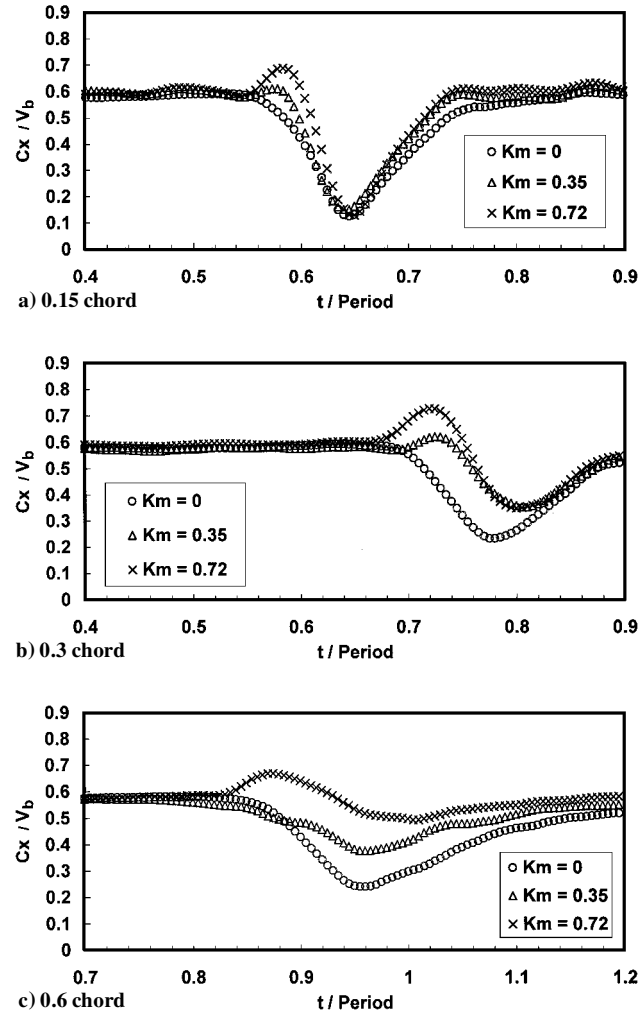

Fig. 5 Measured axial velocity wake profile with hot wire located aft of the rotor trailing edge at high blade loading.

except that a substantial portion of the energized wake has attained higher momentum in contrast to that of Fig. 4a. (The entire wake is right shifted in time due to the rotor stagger angle.) At 60% chord aft, Fig. 4c suggests that the surplus momentum of the injected flow has diffused across the wake, with greater blowing momentum resulting in a smaller net velocity deficit. Note that the abscissa of Fig. 4c is right shifted.

Wake profiles at high loading ($C_x/V_b = 0.53$), just before the onset of rotating stall, are presented in Figs. 5a–5c. At the 15% chord location (Fig. 5a), the maximum velocity defect with or without blowing flow is approximately the same. This suggests that the injected flow has not yet impacted the base flow (no blowing case, $K_m = 0$). This is understandable because the velocity defect at high loading is much more severe than the near-design case of $K_m = 0$) (Fig. 4a). At 30% chord aft of the trailing edge, Fig. 5b shows that the effect of the blowing flow on the velocity defect can be clearly seen. Farther downstream at 60% chord, similar to that of Fig. 4c, Fig. 5c suggests that the different rate of blowing flow has a distinct impact on the wake velocity defect. The abcissa of Fig. 5c is right shifted.

B. Gust factor

The gust factor G, discussed in Sec. III, allows one to access the effect of flow injection on transverse gust (Fig. 2). With velocity profiles measured, the gust factor can now be calculated, as shown in Fig. 6 for all blowing cases tested. Results clearly show that as the blowing momentum defect factor K_m increases, due to the increase

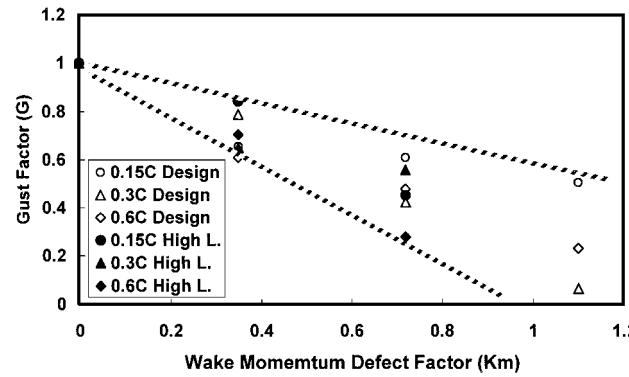

Fig. 6 Gust factor vs wake momentum defect factor over the entire range of data taken.

in blowing mass flow, the gust factor G decreases, which is the case for both loading levels. The two shaded lines define the bounds of the overall trend of monotonic decrease in the gust factor. With these data at hand, one can expect a decreased unsteady loading on the stator because the unsteady loading is mainly due to the upstream wake.

C. Unsteady Loading on Stator

With the upstream rotor wake well quantified, its effect on the downstream stator row can now be accessed. Figure 7 presents

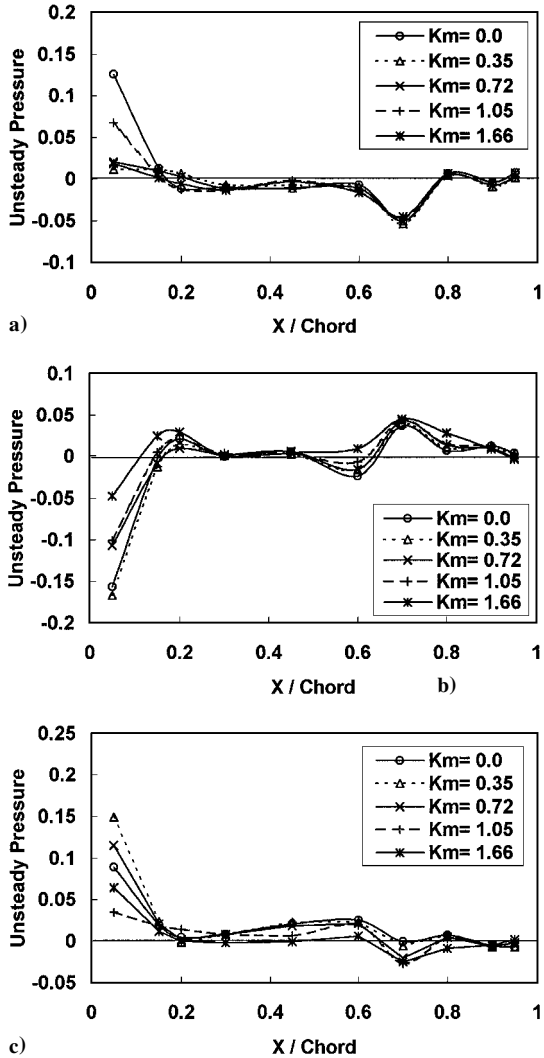

Fig. 7 Chordwise distribution of normalized unsteady pressure on the stator suction surface with various blowing flow at normalized time of a) $t/T = 0.0$, b) $t/T = 0.4$, and c) $t/T = 0.8$.

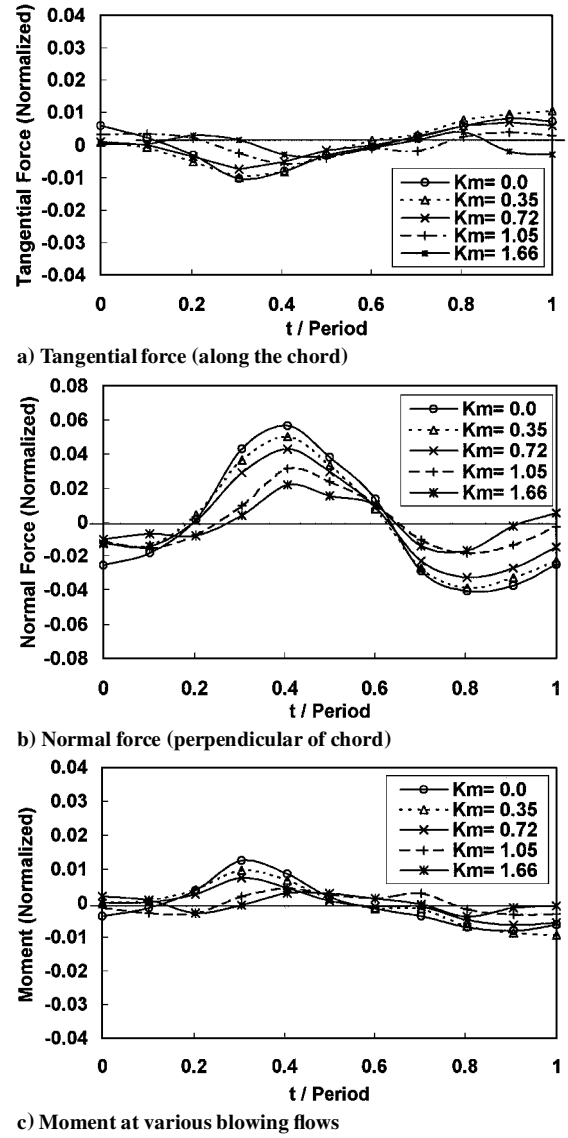

Fig. 8 Excursion of stator.

the chordwise variation of ensemble-averaged unsteady pressure signature along the stator suction surface for all blowing flow rates at near-design loading. (The unsteady pressure amplitude on the pressure surface is essentially zero.) The ordinate, normalized unsteady pressure is defined as

$$\tilde{p}/0.5\rho V_b^2$$

where $\tilde{p}$ is the local unsteady pressure (instantaneous pressure minus the time-mean) and V_b is the blade velocity. Data are presented for three time intervals within an unsteady cycle-normalized time $t/T = 0.0$, 0.4, and 0.8. The results at other times add little physical significance to that shown.

Figure 7 suggests that for all blowing flows the largest unsteadiness in pressure occurs at the forward portion of the blade chord, with the rest of the blade having a local normalized pressure fluctuation of only a few percent. The unsteady pressure fluctuation near the leading edge naturally will dominate the unsteady forced response. The large pressure excursion is also demonstrated by Hsu and Wo,[7] who went one step further and showed that the maximum departure from the mean pressure occurs at the time when the upstream wake meets the stator suction surface near the leading edge.

Valkov and Tan[4] provide an excellent physical insight for this behavior, thanks to their spectral code, which is able to capture fine flow features. Their Navier–Stokes results of upstream wake impinging on the stator cascade show that, as the wake interacts with the blade boundary-layer, B vortices are being ejected from the boundary layer into the outer flow a few boundary layer thickness from the blade surface. As these B vortices are convected downstream, they induce a large pressure fluctuation on the surface. The present data show that this effect is important near the leading-edge region and decays rapidly downstream. However, hot-wire measurement near the stator leading edge is not available to definitively link their calculated result with the data.

Figure 8 shows the excursion of unsteady force, integrated from the data of Fig. 7, on the stator for all cases of blowing mass flow considered at near-design loading. The ordinates for Figs. 8a, 8b, and 8c represent, respectively, nondimensional unsteady force tangent to the blade chord, $\tilde{F}_t/0.5\rho C V_b^2$; the nondimensional unsteady force normal to the blade chord, $\tilde{F}_n/0.5\rho C V_b^2$; and the nondimensional unsteady moment about the midchord, $\tilde{M}/0.5\rho C^2 V_b^2$. These three unsteady quantities, obtained from integrating the unsteady pressure data (instantaneous pressure minus time mean), thus include all harmonic components. Note that the force normal to the chord (Fig. 8b) exhibits the largest unsteady amplitude (note the expanded scale for Figs. 8a and 8c), with the amplitude of tangential force and moment less than 2%. This confirms that the transverse gust v^+ is more important than the streamwise gust u^+ (see Fig. 2). Intuitively, the transverse gust is more important than the streamwise gust because it is the transverse gust, which in essence acts in the direction normal to the blade chord, that contributes most to $\tilde{F}_n$. This will still be the case even if u^+ and v^+ are equal in magnitude. The maximum amplitude in Fig. 8b with uncontrolled wake ($K_m = 0$) is about 6%,

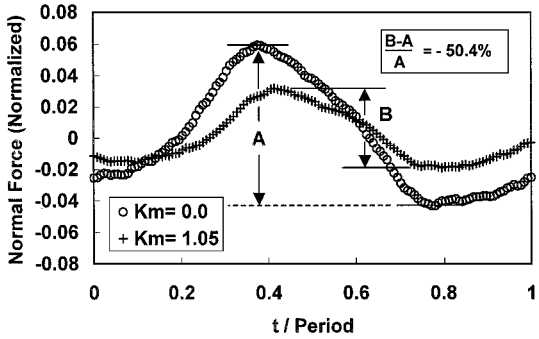

Fig. 9 Force reduction factor $(B - A)/A$, defined to quantify the reduction of stator unsteady force with blowing compared to the no blowing case (K_m) = 0.

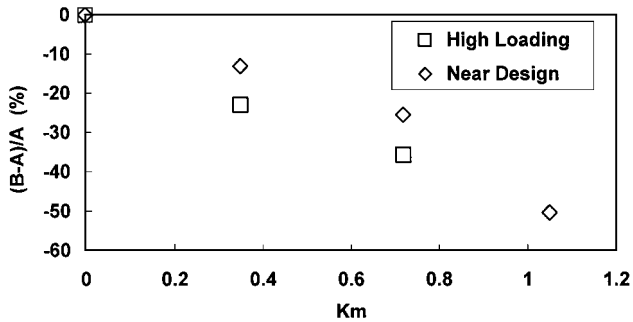

Fig. 10 Reduction of unsteady force amplitude on the stator over a range of blowing flows for two blade time-mean loadings (definition of ordinate in Fig. 9).

which is the largest for all cases examined, with the magnitude decreasing with increasing blowing flow. Data at high loading also exhibit the same qualitative trend.

To interpret the data further, one needs to quantify better the reduction of unsteady loading as a result of flow control. Figure 9 shows a typical excursion of unsteady loading where the peak-to-peak amplitude without blowing, A is subtracted from the blowing case, B, and presented as a percentage change reference to the no blowing case, defined as the force reduction factor $(B - A)/A$. Figure 10 presents this force reduction factor over the range of wake momentum defect factor K_m with control. An essentially linear relationship between the two factors for all cases tested suggests that trailing-edge blowing technique is effective in decreasing unsteady loading due to gust over a broad range of wake profiles and time-mean blade loading. At the largest value of K_m tested, reduction in the unsteady force is still achieved. (However, it is reasonable to believe that excessive blowing would become a source of gust rather than reducing it.) This methodology seems to be insensitive to the manner in which injection occurs because, as mentioned, the blowing air trajectory is quite biased toward the pressure surface (see Figs. 4 and 5). It seems reasonable that the rate of mixing, however, would depend on details of the flow control geometry. In other words, modification of blowing nozzle design should affect the development of wake profile downstream. Nevertheless, the force reduction achieved is a welcomed result.

Figure 11 links the gust factor G to the force reduction factor $(B - A)/A$. Without control the gust is largest, $G = 1$, with no force reduction, $(B - A)/A = 0$. The overall trend shows monotonic decrease in force with gust factor, consistent with the results of Fig. 6. Note that the magnitude of force reduction factor is quite substantial. These data suggest that so long as one can decrease the transverse gust, by whatever means of flow control, reduction in forced response will occur. It might be that the quantitative result of Fig. 11 is independent of flow control strategy used, however, further testing is required to justify this claim.

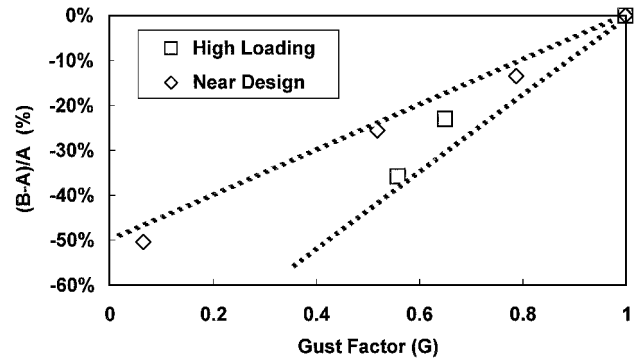

Fig. 11 Reduction of stator unsteady force amplitude vs gust factor, with variation of gust factor due to blowing flows; shaded lines show the bounds of the data. [See Eq. (3) for definition of abscissa and Fig. 9 for the ordinate.]

VI. Conclusions

This paper addresses flow control via rotor trailing-edge blowing in a rotor/stator axial compressor with 30% chord axial spacing between blade rows and two time-mean blade loadings. Focuses are the wake characteristics resulting from various blowing amounts and their effect on the unsteady gust response of the downstream stator.

With the present flow control scheme, the development of the near wake is shown to be very much load dependent. At 15% chord, a given amount of blowing momentum has an affect on the velocity defect at near-design loading but not at high loading (compare Fig. 4a with Fig. 5a). This suggests that the effectiveness of a particular flow control scheme is dependent on details of how and where evaluation is made. Wake data for both loadings taken at 30% chord (Figs. 4b and 5b) show clear reduction in the velocity defect. Generally, beyond the near-wake region, increase in the blowing flow momentum would result in further decrease in the rotor wake velocity defect.

Calculation of the gust factor G based on the wake data show that the gust factor indeed decreases with wake momentum defect factor K_m (Fig. 6). This suggests that reduction in the stator forced response is guaranteed, which is indeed shown to be the case (Figs. 8 and 10). Near-linear decrease of stator unsteady force with increase in blowing momentum is evident (Fig. 10). In hindsight, this relationship perhaps can be expected because the level of unsteady force is in the linear range (maximum force amplitude of about 6%, Fig. 8b) and increase in blowing flow should result in near-linear decrease in forced response. This should hold until the injected flow itself became a source of gust.

Acknowledgment

The authors are grateful for the financial support of the National Science Council (NSC), Republic of China (Grant NSC 89-2612-E-002-002).

References

[1] Park, W. J., and Cimbala, J. M., "Effect of Jet Injection Geometry on Two-Dimensional Momentumless Wakes," *Journal of Fluid Mechanics*, Vol. 224, March 1991, pp. 29–47.

[2] Kerrebrock, J. L., Drela, M., Merchant, A. A., and Schuler, B. J., "Family of Designs for Aspirated Compressors," American Society of Mechanical Engineers, ASME Paper 98-GT-196, June 1998.

[3] Rao, N. M., Feng, J., Burdisso, R. A., and Ng, W. F., "Experimental Demonstration of Active Flow Control to Reduce Unsteady Stator–Rotor Interaction," *AIAA Journal*, Vol. 39, No. 3, 2001, pp. 458–464.

[4] Valkov, T., and Tan, C. S., "Control of the Unsteady Flow in a Stator Blade Row Interacting with Upstream Moving Wakes," *Journal of Turbomachinery*, Vol. 117, No. 1, 1995, pp. 97–105.

[5] Waitz, I. A., Brookfield, J. M., Sell, J., and Hayden, B. J., "Preliminary Assessment of Wake Management Strategies for Reduction of Turbomachinery Fan Noise," *Journal of Propulsion and Power*, Vol. 12, No. 5, 1996, pp. 958–966.

[6]Manwaring, S. R., and Wisler, D. C., "Unsteady Aerodynamics and Gust Response in Compressors and Turbines," *Journal of Turbomachinery*, Vol. 115, No. 4, 1993, pp. 724–740.

[7]Hsu, S. T., and Wo, A. M., "Reduction of Unsteady Blade Loading by Beneficial Use of Vortical and Potential Disturbances in an Axial Compressor with Rotor Clocking," *Journal of Turbomachinery*, Vol. 120, No. 4, 1998, pp. 705–713.

[8]Wo, A. M., Chung, M. H., and Hsu, S. T., "Gust Response Decomposition in a Stator/Rotor Axial Compressor with Varying Axial Gap," *Journal of Propulsion and Power*, Vol. 13, No. 2, 1997, pp. 178–185.

[9]Hobbs, D. E., and Weingold, H. D., "Development of Controlled Diffusion Aerofoils for Multistage Compressor Applications," *Journal of Engineering for Gas Turbine and Power*, Vol. 106, No. 2, 1984, pp. 271–278.

[10]Greitzer, E. M., "An Introduction to Unsteady Flow in Turbomachines," *Thermodynamics and Fluid Mechanics of Turbomachinery*, edited by A. S. Ucer, P. Stow, and C. Hirsch, Vol. 2, *Proceedings of the NATO Advanced Study Institute*, Dordrecht, The Netherlands, 1984, p. 989.

[11]Doebelin, E. O., *Measurement Systems: Application and Design*, 4th ed., McGraw–Hill, New York, 1990, p. 482.

[12]Hsu, S. T., and Wo, A. M., "Near-Wake Measurement in a Rotor/Stator Axial Compressor Using Slanted Hot-Wire Technique," *Experiments in Fluids*, Vol. 23, 1997, pp. 441–444.